ISSN 2076-2429 (print)
ISSN 2223-3814 (online)

UDC 621.575.932:621.565.92

O. Titlov, DSc., Prof.,
K. Ponomaryov
Odesa National University of Technology, 112 Kanatna Str., Odesa, Ukraine, 65039; titlov1959@gmail.com

SIMULATION OF THERMAL MODES OF THE ABSORPTION THERMOTRANSFORMER WITH HEAT PIPES

О. Тітлов, К. Пономарьов. **Моделювання теплових режимів абсорбційного термотрансформатора з тепловими трубами.** Запропоновано методику моделювання теплових режимів абсорбційного термотрансформатора з тепловими трубами, яка дозволяє за рахунок раціонального компонування конструкції покращити його температурно-енергетичні характеристики. Розроблено математичну модель теплової схеми «випарник абсорбційного термотрансформатора – теплова труба – об'єкт охолоджування», що дозволяє проводити чисельний експеримент з оцінки впливу на температурно-енергетичні характеристики абсорбційного термотрансформатора, а саме короба об'єкта охолоджування, наступних геометричних та режимних параметрів: глибини, ширини та висоти короба об'єкта охолоджування; товщини матеріалу короба об'єкта охолоджування; типу матеріалу короба; типу використаної теплової труби з урахуванням величини теплового опору; товщини теплоізоляційних перегородок. В основі методики розрахунку теплових режимів лежить рівняння теплового балансу, яка враховує холодопродуктивність випарника абсорбційного термотрансформатора, надходження теплоти з навколишнього середовища через стінки шафи, через двері та перегородки, а також надходження тепла від продуктів. Варійованими параметрами були: товщина коробу – 0,003 м та 0,001 м; висота коробу – 0,160 м, 0,200 м, 0,280 м; глибина коробу – 0,225 м, 0,325 м, 0,425 м; термічний опір теплових труб – 0,01 К/Вт, 0,1 К/Вт, 1 К/Вт. Базовими конструкціями для аналізу є короби з Г-подібними, П-подібними та традиційними тепловими трубами. В результаті чисельного експерименту доведено, що для розміру об'єкта охолоджування: висота – 0,160 м, ширина – 0,385 м, глибина 0,225 м, встановлення теплової труби вирівнює температури до 0,2 °С. Вихід на режим здійснюється швидше приблизно на 20%. Зростання глибини коробу від 0,225 м до 0,425 м знижує ефективність застосування теплових труб на 45%, а збільшення висоти з 0,160 м до 0,280 м знижує ефективність використання теплових труб на 2,6%. Для розробників абсорбційних термотрансформаторов з корисним об'ємом об'єкта охолоджування 12...30 дм^3 та 100...180 дм^3 можливо рекомендувати конструкцію коробу з габаритами 0,160×0,225×0,385 мм, і з тепловими трубами Г-подібного або П-подібного типу. Теплоносій теплових труб – аміак.

Ключові слова: абсорбційний термотрансформатор, теплова труба, тепловий режими, моделювання, тепловий баланс

O. Titlov, K. Ponomaryov. **Simulation of thermal modes of the absorption thermotransformer with heat pipes.** Methodology for thermal regimes simulation of absorption thermotransformer with heat pipes is proposed, which, through rational structural construction design, improves its thermal and power performance. Mathematical model has been developed for the thermal system comprising the "absorption thermotransformer evaporator – heat pipe – cooling object", which enables numerical experiments to evaluate the influence of the following geometric and operating parameters, namely: depth, width, and height of the cooling facility enclosure; thickness of the cooling facility enclosure material; type of enclosure material; type of heat pipe used, taking into consideration its thermal resistance; and thickness of the thermal insulation barriers on the thermal and power characteristics of the absorption thermotransformer, specifically, the cooling facility enclosure. The basis of the thermal modes calculation methodology is the thermal balance equation, which accounts for the absorption thermotransformer evaporator cooling capacity, heat transfer from the surrounding environment through the cabinet walls, doors, and barriers, as well as heat input from the stored products. The varied parameters included: enclosure thickness – 0.003 m and 0.001 m; enclosure height – 0.160 m, 0.200 m, 0.280 m; enclosure depth – 0.225 m, 0.325 m, 0.425 m; and thermal resistance of the heat pipes – 0.01 K/W, 0.1 K/W, 1 K/W. The baseline designs for analysis were enclosures with L-shaped, U-shaped, and conventional heat pipes. As a result of the numerical experiment, it was proven that for a cooling object size of height – 0.160 m, width – 0.385 m, and depth – 0.225 m, the installation of a heat pipe equalizes temperatures to within 0.2 °C. The operating mode is reached approximately 20% faster. Increasing the depth of the enclosure from 0.225 m to 0.425 m reduces the efficiency of heat pipe usage by 45%, while increasing the height from 0.160 m to 0.280 m reduces efficiency by 2.6%. For developers of absorption thermotransformers with cooling object net capacity 12…30 dm^3 and 100…180 dm^3, the recommended enclosure design is with dimensions of 0.160×0.225×0.385 m, and with L-shaped or U-shaped heat pipes. The working fluid of the heat pipes is ammonia.

Keywords: absorption thermotransformer, heat pipe, thermal modes, simulation, thermal balance

Introduction

The transition of low-temperature cooling systems to environmentally safe refrigerants necessitates increased attention to absorption thermotransformers, whose working fluid consists of natural components – water-ammonia solution and inert gas [1].

Absorption thermotransformers possess several advantageous characteristics, such as noiseless operation, reliability, and long service life, as well as the absence of vibration, magnetic, and electric fields during operation. They also offer the capability to utilize multiple energy sources – both electrical and thermal – within a single unit. Absorption thermotransformers are relatively insensitive to variations in power supply parameters within a voltage range of 160…240 V [2].

DOI: 10.15276/opu.1.71.2025.05

Among the advantages of absorption thermotransformers is their lower cost compared to compression-type counterparts, which is often a decisive factor. Absorption thermotransformers are effective in applications such as mini-refrigerators, minibars, and built-in or transport refrigerator models, where cooling capacity does not exceed 20 W, making the use of compression cooling systems impractical.

At the same time, absorption thermotransformers exhibit higher energy consumption compared to equivalent compression models, which limits their range of application [3].

Therefore, research aimed at improving the energy efficiency of absorption heat pumps remains highly relevant.

One promising direction in such research is the development of efficient thermal coupling between the cooling object and the artificial cold source (absorption thermotransformers evaporator) using heat pipes [4, 5].

Currently, there are practical implementations of such systems [1], yet comprehensive models that can provide guidance for the design of various types of cooling systems are lacking.

Analysis of literary data and statement of the problem

Based on the experience of foreign and domestic developers [2, 4, 5], it is advisable to adopt the three-flow heat exchanger scheme shown in Fig. 1 as the basic model of the evaporator (artificial cold source) of the absorption thermotransformer (absorption thermotransformers).

The heat exchanger-evaporator consists of a liquid ammonia pipe *1*, thermally connected to the evaporator pipe *2*. Coaxially within the evaporator is a channel for the purified vapor-gas mixture *3*. Radial capillary grooves *4* are applied to the inner surface of the evaporator pipe. Liquid ammonia, entering the upper part of the evaporator due to the hydrostatic column, flows countercurrently to the lower part. The capillary grooves *4*, owing to surface tension forces, distribute the liquid ammonia film evenly along the entire internal perimeter of the evaporator *2*. Ammonia from both the stream and the grooves evaporates into the vapor-gas mixture due to the difference in partial pressures between the flow and the liquid film surface. This evaporation process produces artificial cold at a temperature below ambient. The evaporation temperature level is determined by the heat and mass transfer requirements between ammonia and the vapor-gas mixture, the degree of vapor-gas mixture purification, the circulation rate, and the geometric characteristics of the evaporator *2* and heat exchanger elements (*1* and *3*) [5, *6*, 7].

To ensure serviceability, both the absorption thermotransformers and the heat pipes must be designed as detachable assemblies.

A well-established technical solution exists for the installation and positioning of the absorption thermotransformers evaporator entirely within a thermal insulation block [8]. The block is located in the rear opening of the insulated cabinet. The evaporator is non-detachably installed inside the block (via polyurethane foam insulation) and is structurally connected at several straight segments to the block base made from a highly thermally conductive metal, such as aluminum.

The design layout is shown in Fig. 2.

The insulated cabinet 1 with doors *2* is divided into a low-temperature compartment *3* and a refrigeration chamber *4*. The low-temperature compartment *3* has a separate door *5* and is designed as an enclosure *6* made of a highly thermally conductive material, e.g., aluminum. The enclosure *6* is connected to the cabinet *1* using detachable joints.

The absorption thermotransformers *7* is mounted on the rear wall of the cabinet *1*, with its evaporator *8* fully enclosed in an insulated block *9*. This block *9* is installed in the cabinet opening and, to provide thermal contact with the useful volumes of the cabinet *1*, is equipped with a panel *10* made of a highly thermally conductive material, such as aluminum. The panel *10* is connected via detachable joints to the rear wall of the enclosure *6* through a ribbed plate (panel) *11* located on the rear wall of the refrigeration chamber *4*.

The ribbed panel can also be fabricated as a single unit with panel *10*. Heat pipes *12* are installed within the low-temperature compartment: the heat pipe condenser is mounted on the rear wall of the enclosure *6*, and the evaporator – on the side wall.

Analysis of known experimental studies of absorption thermotransformers systems based on the scheme shown in Fig. 2 demonstrates that the thermal mode of the refrigeration chamber *4* can be calculated without significant complications using existing methodologies for finned surfaces and panels [5, 9].

ISSN 2076-2429 (print)
ISSN 2223-3814 (online)

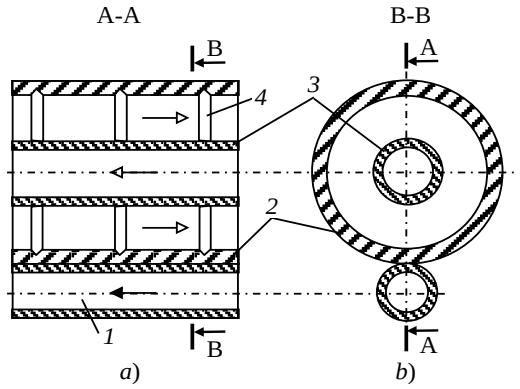

Fig. 1. Scheme of the three-flow evaporator absorption refrigeration devices: *a*) longitudinal section of a straight section; *b*) cross-section of a straight section

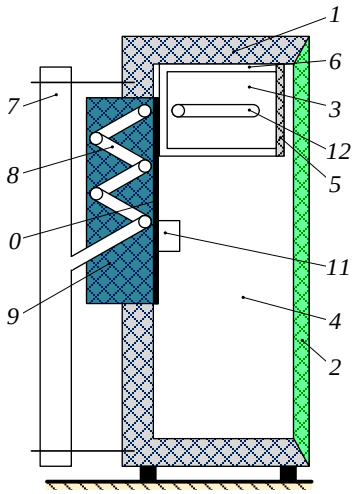

Fig. 2. Diagram of the basic design of an absorption thermal transformers with heat pipes

However, it should be noted that the mass and size characteristics of the ribbed panel *11* are not strictly limited due to the relatively large volume of the refrigeration chamber *4*.

The purpose and objectives of the research

The aim of this work is to simulate the thermal modes of absorption thermotransformers (absorption thermotransformers).

Analysis of the absorption thermal transformers thermal scheme

The greatest difficulty in the calculations arises from the thermal coupling between the absorption thermotransformers evaporator and the low-temperature compartment enclosure via the heat pipes.

The general thermal diagram of this heat connection is presented in Fig. 3.

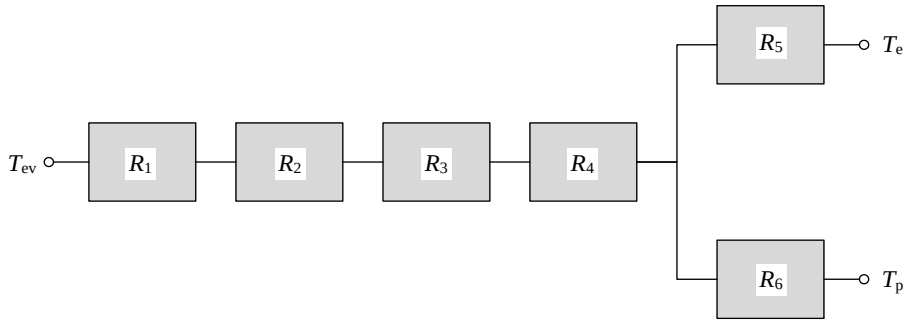

Fig. 3. Thermal scheme: Tempreture: T_{ev} – of the evaporator; T_e – of the ambient air; T_p – of the stored products; Thermal resistance: R_1 – of the evaporator wall; R_2 – of the contact between the evaporator and the plate of the insulated block; R_3 – of the contact between the plate of the insulated block and the rear wall of the RC box; R_4 – of the box walls; R_5 – of the refrigerator cabinet; R_6 – of the convective heat exchange process with products

When installing heat pipes, the thermal resistance of the enclosure can be expressed as:

$$\frac{1}{R_4}=\frac{1}{R_s}+\frac{1}{R_{hp}}, \tag{1}$$

where: R_4 – total thermal resistance of the enclosure, K/W; R_s – thermal resistance of the enclosure walls, K/W; R_{hp} – thermal resistance of heat pipes, K/W.

To develop a mathematical model, it is necessary to assess the influence of various factors under the conditions of real operating modes of the absorption thermal transformers. Based on this assessment, assumptions and boundary conditions can be formulated.

The heat balance equation in general form for the low-temperature volume, presented in Figure 4 and Figure 5, has the following form:

$$Q_0 = Q_e + Q_{rc}^{(1)} + Q_{rc}^{(2)} + Q_p, \quad (2)$$

where: Q_e – heat input from the environment through the refrigeration chamber cabinet walls, W; $Q_{rc}^{(1)}$, $Q_{rc}^{(2)}$ – heat input from the refrigeration chamber through the low-temperature compartment doors and barrier, W; Q_p – heat input from stored products, W.

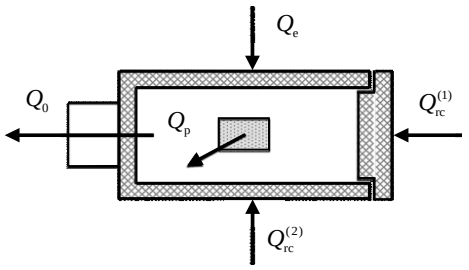

Fig. 4. Heat flow balance of the low-temperature compartment, expressed in general form

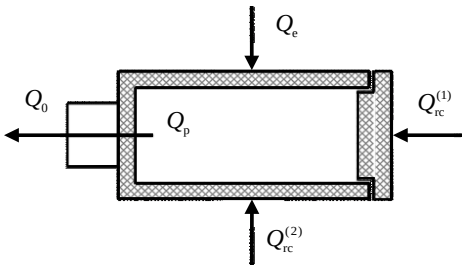

Fig. 5. Heat flow balance in long-term product storage mode

In stationary long-term storage mode $Q_p = 0$. Thus, equation (2) will take the form:

$$Q_0 = Q_e + Q_{rc}^{(1)} + Q_{rc}^{(2)}. \quad (3)$$

For a two-chamber cabinet with separate doors for the lower heat exchange volume and the refrigerator compartment $Q_{rc}^{(1)}$ is included in Q_e.

Equations (2) and (3) are written for the stationary mode of operation of the absorption thermal transformers. This “extended” mode corresponds to peak thermal loads, which occur when ambient air temperature reaches 32 °C or higher – representing the most unfavorable (critical) operating conditions for the absorption thermotransformers.

The thermal connection scheme, taking into account the assumptions made, is shown in Figure 6.

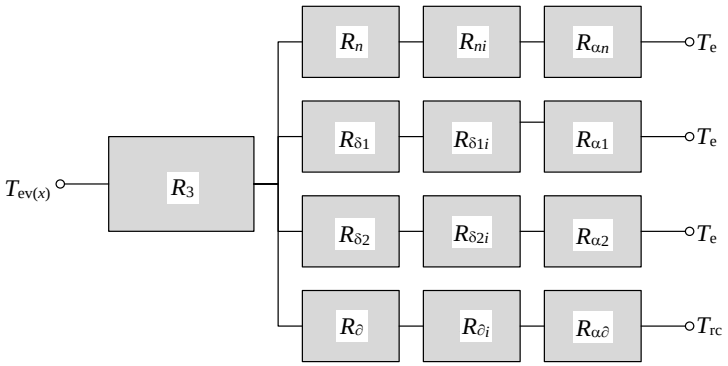

Fig. 6. Thermal scheme: $T_{ev(x)}$ – temperature distribution along the length of the evaporator; T_e – environmental temperature; T_{rc} – temperature in refrigeration chamber; Thermal resistance: R_3 – of the back wall of the box; R_n – of the wall of the ceiling of the box; $R_{\delta 1}$ – of the side wall connected to the initial section of the evaporator; $R_{\delta 2}$ – of the side wall connected to the final section of the evaporator; R_∂ – of the box bottom wall; R_{ni} – of the insulation of the cabinet lid; $R_{\partial 1i}$, $R_{\partial 2i}$ – of the insulation of the side walls of the cabinet; $R_{\alpha 1}$, $R_{\alpha 2}$ – of the convective heat exchange process on the side walls of the cabinet; $R_{\alpha\partial}$ – of the convective heat transfer process on the partition

An analysis of the thermal connection scheme was carried out (Figure 3).

ISSN 2076-2429 (print)
ISSN 2223-3814 (online)

Thermal resistance R_1 and R_2 are difficult to calculate precisely due to a large number of technological factors, such as non-planarity and misalignment during assembly, tightening torque of threaded joints, and other fabrication and installation features.

The influence of these factors can be partially mitigated using known methods of enhancing heat transfer in the contact zone – for example, by installing highly porous cellular materials with a copper-based frame or applying thermally conductive pastes [4].

In this case, it is necessary to adjust boundary conditions based on experimental research results. At the initial stage, when formulating assumptions, a linear temperature distribution along the evaporator length can be assumed.

The assessment of the thermal resistance of the enclosure wall in the direction of the heat flow shows that its value is practically zero. The value R_4, which characterizes the thermal resistance of the walls of the lower heat exchange volume box during conductive heat transfer, is taken to be zero in the first approximation, i.e. the heat pipe is considered to have infinitely high thermal conductivity.

When the lower heat exchange volume is loaded with products, convective heat inflows through the low-temperature volume doors are practically zero, i.e.: $R_7 = \infty$, $Q_{\text{rc}}^{(1)} = 0$.

The directions of heat flows are shown in Figure 7.

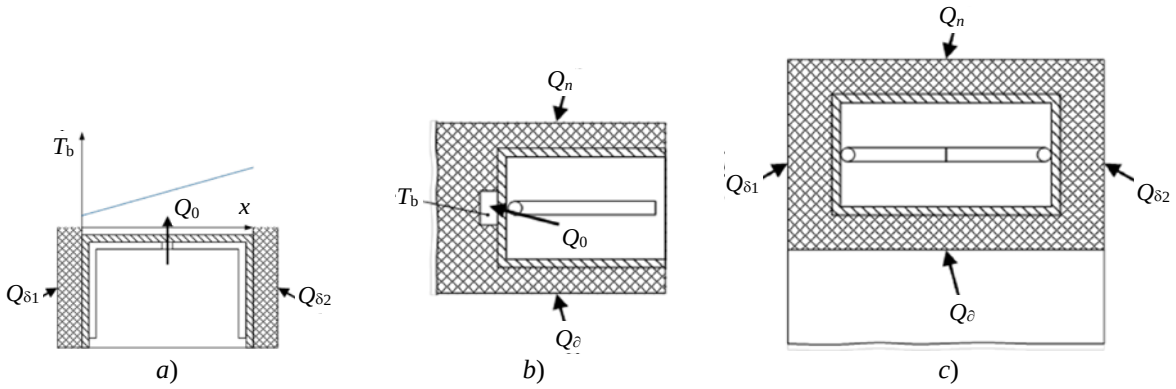

Fig. 7. Directions of heat flows on the model diagram of thermal communication:
a) top view; *b*) side view; *c*) front view

We also assume the temperature in the low-temperature volume to be constant and equal to T_0. The following balance of heat flows corresponds to the formulated assumptions:

$$Q_0 = Q_e + Q_{rc}^{(2)}. \tag{4}$$

Equation (4), taking into consideration the accepted designations, can be written in the following form:

$$Q_0 = Q_p + Q_\partial + Q_{\delta 1} + Q_{\delta 2}. \tag{5}$$

According to the adopted scheme, the heat supply to the evaporator occurs in the mode of convective heat exchange through the walls of the low-temperature volume enclosure.

The heat pipe, taking into account the assumption of infinite thermal conductivity, acts as a kind of isothermal axis that penetrates the walls of the enclosure.

Mathematical model of the heat balance of the elementary cell of the low-temperature volume box

The mathematical model of thermal couplings is based on the heat balance of an elementary representative cell of the low-temperature compartment enclosure:

a) the elementary cell is not in direct contact with the heat pipe (see Fig. 8).

The change in the thermal regime of the elementary cell (or the change in its internal energy) can be expressed as follows:

$$\Delta Q_{i,j} = \Delta Q_{i,j+1} + \Delta Q_{i,j-1} + \Delta Q_{i-1,j} + \Delta Q_{i+1,j} + Q_{in(i,j)}, \tag{6}$$

where: $Q_{in(i,j)}$ – the heat flow into the elementary cell from the surrounding environment, or, in the case where the elementary cell is located at the bottom of the enclosure, from the refrigeration chamber.

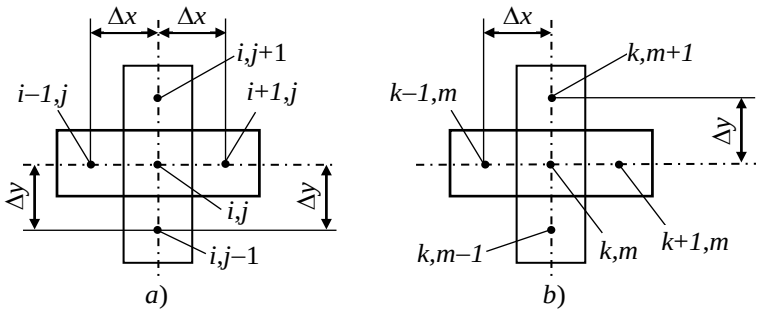

Fig. 8. Elementary cells: *a*) of the first type; *b*) of the second type

Equation (6) is written based on the assumption that there is no thermal influence from the stored products.

It is also assumed that $Q_{in(i,j)} = 0$, when the elementary cell is located on the rear wall of the enclosure and is in direct thermal contact with the absorption thermotransformers evaporator. In other words, there are no heat inflows into the low-temperature volume from the absorption thermotransformers evaporator, which is justified, since the evaporator acts as a "heat sink" from the low-temperature volume.

Alternatively, the change in the thermal regime of the elementary cell can be described using a known method [10]:

$$dQ_{i,j} = C_{i,j} \cdot \rho_{i,j} \left(\frac{dt}{d\tau} \right)_{i,j} \cdot dV_{i,j}, \tag{7}$$

where: $C_{i,j}$ and $\rho_{i,j}$ – heat capacity and density of the elementary cell material; $dV_{i,j}$ – elementary cell volume; $\left(\frac{dt}{d\tau} \right)_{i,j}$ – change in elementary cell temperature over time.

Equation (7) can also be expressed using finite increments:

$$\Delta Q_{i,j} = C_{i,j} \cdot \rho_{i,j} \left(\frac{\Delta t}{\Delta \tau} \right)_{i,j} \cdot V_{i,j}. \tag{8}$$

By transforming equation (8), we can obtain a convenient notation form for calculation:

$$\Delta t_{i,j} = \frac{\Delta \tau}{C_{i,j} \cdot \rho_{i,j} \cdot V_{i,j}} \cdot \Delta Q_{i,j}. \tag{9}$$

For an elementary cell of the first type, taking into consideration (6), we obtain the basic calculation formula for the elementary cell:

$$\Delta t_{i,j} = \frac{\Delta \tau}{C_{i,j} \cdot \rho_{i,j} \cdot V_{i,j}} \cdot (\Delta Q_{i,j+1} + \Delta Q_{i,j-1} + \Delta Q_{i-1,j} + \Delta Q_{i+1,j} + Q_{in(i,j)}). \tag{10}$$

A similar formula can be written for the elementary cell of the insulating coating:

$$\Delta t_{\text{p,q}} = \frac{\Delta \tau}{C_{\text{p,q}} \cdot \rho_{\text{p,q}} \cdot V_{\text{p,q}}} \cdot \Delta Q_{\Sigma(\text{p,q})} \tag{11}$$

b) the elementary cell is in thermal contact directly with the evaporator or condenser of the heat pipe (Fig. 8).

In this case, equation 6 can be expressed in the following form:

$$\Delta Q_{k,m} = \Delta Q_{k,m+1} + \Delta Q_{k,m-1} + \Delta Q_{k-1,m} + \Delta Q_{k+1,m} + Q_{\text{hp}(k,m)}, \tag{12}$$

where: $Q_{\text{hp}(k,m)}$ – value of the heat flow introduced (or removed) by the heat pipe into (from) the elementary cell, W.

The signs "+" or "–" allow us to determine the direction of the heat flow in equation (11).

ISSN 2076-2429 (print)
ISSN 2223-3814 (online)

Similarly, from equations (8) and (9) we can obtain an expression for the second type of elementary cells:

$$\Delta t_{k,m} = \frac{\Delta\tau}{C_{k,m} \cdot \rho_{k,m} \cdot V_{k,m}} \xi \Delta Q_{k,m} = \Delta Q_{k,m+1} + \Delta Q_{k,m-1} + \Delta Q_{k-1,m} + \Delta Q_{k+1,m} \pm Q_{\text{in}(k,m)} \pm Q_{\text{hp}(k,m)}. \quad (13)$$

For each elementary cell of the low-temperature cooling enclosure, as well as for the elementary cell of the insulating coating in the low-temperature cooling area, it is necessary to write down a system of equations of the type (10) and (13):

$$\left.\begin{aligned} \Delta t_{k,m} &= \frac{\Delta\tau}{C_{k,m} \cdot \rho_{k,m} \cdot V_{k,m}} \cdot \Delta Q_{\Sigma(k,m)}; \\ \Delta t_{i,j} &= \frac{\Delta\tau}{C_{i,j} \cdot \rho_{i,j} \cdot V_{i,j}} \cdot \Delta Q_{\Sigma(i,j)}; \\ \Delta t_{p,q} &= \frac{\Delta\tau}{C_{p,q} \cdot \rho_{p,q} \cdot V_{p,q}} \cdot \Delta Q_{\Sigma(p,q)} \end{aligned}\right\}. \quad (14)$$

The solution of equation 14, expressed in the form of finite-difference relations, is carried out by known numerical methods. The most common is the Euler method [11].

The boundary conditions for equation (14) have the following form:

– the initial temperature in the elementary cell of the enclosure and insulation at the time $\tau = 0$;

– ambient temperature (room air temperature);

– temperature at the “cold” point, i.e., the temperature of the heat-receiving source.

Specifying time increment $\Delta\tau_1$, the temperature value at a point in time is calculated: $\tau_1 = \tau_0 + \Delta\tau_1$. The obtained values form an array of parameters that serves as the basis for the next time increment $\Delta\tau_2$, so $\tau_2 = \tau_1 + \Delta\tau_2$.

Calculations are performed until temperatures that meet specified boundary conditions or convergence criteria are reached.

The right choice $\Delta\tau$ and Δt when solving systems of finite-difference equations has a significant value. When using explicit (type 14) finite-difference schemes, the value of the permissible time step is limited and for internal nodes it depends on the size of the chosen step in the spatial coordinate and the thermal conductivity of the material $\alpha = \lambda / \rho \cdot c$. It is recommended [11] that:

$$\alpha \frac{\Delta\tau}{\Delta x^2} = 1.2, \quad (15)$$

but when the value of the complex is greater than 1.2, instability occurs, which is not related to rounding errors and is a property of the system of finite-difference equations itself.

The search (choice) of the temperature of the “cold” source, which is a function of the absorption-diffusion refrigeration unit evaporator performance, as well as the heat exchange conditions in the contact zone, should be considered an important point in the part of setting the boundary conditions.

The value of the thermal resistance can be calculated using the method [12]. the calculation formula has the following form:

$$\frac{1}{R_c} = \frac{2}{3}\lambda_c \left[\frac{2}{3}(1-\varphi_k) h_i + (h_1 - h_2)(1-\varepsilon_k) \right], \quad (16)$$

where: λ_c – thermal conductivity of the material; h_1 and h_2 – the size of the microprotrusions of the contacting surfaces, m; ε_k – change in elementary cell temperature over time; $\varphi_k = F_f / F_i$; F_f, F_i – surface area of contacting pairs, m^2:

$$\varepsilon_k = \frac{4}{\pi(h_1 + h_2)} \cdot \frac{P}{l} \left[\frac{1-\mu_1^2}{E_1} \left(\ln \frac{\alpha}{\varphi_k (1-\varphi_k)} + 0.407 \right) + \frac{1-\mu_2^2}{E_2} \cdot 0.407 \right], \quad (17)$$

where: P – pressing force; E_1 and E_2 – modulus of elasticity of contacting pairs; μ_1 and μ_2 – Poisson's ratios of contacting pairs; l – length of the actual contact area, m.

Analysis of the components of formulas (16) and (17) demonstrates that the total contact thermal resistance depends on the roughness parameters, thermophysical and mechanical characteristics of the contact pair, thermal conductivity of the intercontact medium and the gap arising from the non-planarity of the surfaces.

In addition, the performance characteristics of the three-pass evaporator effect on the temperature of the "cold" source T_0.

The operation process in a three-pass evaporator can be described by a system of differential equations:

$$\left.\begin{aligned} G_0 dY &= \beta(y^* - y)dF; \\ G_0 C'_p dt &= \alpha(t - \vartheta)dF; \\ dQ_0 &= k \cdot \varphi \cdot (\theta - \vartheta)dF = \pm w_0 C_{p0} d\theta \end{aligned}\right\}, \tag{18}$$

where: β – mass transfer coefficient during the evaporation of ammonia into a vapor-gas mixture; α – convective heat transfer coefficient between ammonia and the vapor-gas mixture; k – heat transfer coefficient from ammonia to the object being cooled (low-temperature volume); φ – specific cooling surface area per unit of interfacial contact; θ – temperature in low-temperature volume; t – vapor-gas mixture temperature; ϑ – ammonia saturation temperature; G_0 – inert gas (hydrogen) consumption; w_0 – payload volume low-temperature volume; C_{p0}, C'_p – heat capacity of products in low-temperature volume and inert gas; y – mass fraction of ammonia in vapor-gas mixture; y^* – mass fraction of ammonia in vapor-gas mixture that is in equilibrium with the saturated liquid at a given temperature; Y – mass (relative) fraction of ammonia in vapor-gas mixture; Q_0 – evaporator cooling capacity.

To determine the six unknown parameters (θ, t, ϑ, Y, y, y^*) the system of six equations [13] is formed. Two more necessary equations describe the relationship between y^* and ϑ, and also between y and Y:

$$y = \frac{Y}{1-Y}, \tag{19}$$

$$y^* = A_0 + A_1\vartheta + A_2\vartheta^2 + \cdots + A_n\vartheta^n, \tag{20}$$

where: A_0, A_1, A_2 … A_n – polynomial coefficients.

The sixth equation is the heat balance equation:

$$r\beta(y^* - y)dF = k\varphi(\theta - \vartheta)dF + \alpha(t - \vartheta)dF. \tag{21}$$

The solution of the system of equations (18) – (21) is carried out by the Euler method [11].

The temperature of the "cold" source Q_0 is a boundary condition for the system (14).

However, the value $\vartheta_0 \neq \text{const}$ is defined by the length of the evaporator or by the width of the low-temperature compartment enclosure. In this case, it is necessary to enter $T_0 = \text{const}$, which can be defined, for example, as:

$$T_0 = \frac{\vartheta'_0 - \vartheta''_0}{2}, \tag{20}$$

where: ϑ'_0, ϑ''_0 – temperatures at the beginning and end of the evaporator section, which is connected to the rear wall of the low-temperature cooling enclosure (minimum and maximum).

The basic designs for analysis are enclosures with L-shaped, U-shaped and traditional heat pipes [14, 15].

For the case of using L-shaped and U-shaped heat pipes, the thermal scheme is similar and consists of the following.

The heat pipe evaporators are installed (fixed) on the side walls of the low-temperature volume enclosure, and the condensation areas are on the rear wall of the low-temperature compartment enclosure.

The difference lies in the conditions of heat removal in the condensation zone.

ISSN 2076-2429 (print)
ISSN 2223-3814 (online)

For L-shaped heat pipes, there is an uneven temperature field in the condensation zone. The minimum evaporation temperature will also be the minimum temperature potential for the wall (left) of the low-temperature compartment enclosure. A kind of temperature bias arises between the side walls. However, as shown by a numerical experiment, this value does not exceed 0.8°C for an enclosure wall thickness of 2 mm.

Smoothing (stabilizing) factors when choosing an enclosure with L-shaped heat pipes are partial recondensation of ammonia along the condensation area of the left and right heat pipes. The temperature unevenness on the surface of the low-temperature compartment enclosure rear wall does not exceed 0.5 °C.

For a U-shaped heat pipe, this value does not exceed 0.15 °C.

Thus, in practice, the difference in using L-shaped or U-shaped heat pipes is insignificant. When choosing a thermal scheme, one should proceed from other criteria, for example, from the technological capabilities of the manufacturer. The disadvantage of the low-temperature compartment thermal scheme with two L-shaped heat pipes is the additional costs for double vacuuming, sealing and control of operating parameters.

When manufacturing a low-temperature compartment enclosure with U-shaped heat pipes, these operations are performed only once.

However, an low-temperature compartment enclosure with L-shaped heat pipes offers double reliability in terms of heat pipe failure due to depressurization. The failure of a single L-shaped pipe has a negligible effect on the temperature field of the enclosure, whereas in the case of a U-shaped heat pipe – especially in chambers with a significant flat surface area (up to 40 dm³) – the temperature gradient becomes noticeable and ranges from 2.5 to 2.8 °C.

Rod-type or traditional heat pipe designs in the low-temperature compartment enclosure construction can only be used in cases where temperature field equalization across the wall surfaces is required. This is particularly important for low-temperature compartment with a useful volume of more than 20 dm³, where the characteristic dimensions exceed the following values: 0.3 m – for side walls; 0.46 m – for low-temperature compartment height; 0.66 m – for the width of the enclosure.

Based on the results of numerical experiments, an analysis was carried out on the efficiency of using different types of thermal schemes for enclosures: with L-shaped, U-shaped, and traditional heat pipes.

The variable parameters were: enclosure thickness – 0.003 m and 0.001 m; enclosure height – 0.160 m, 0.200 m, 0.280 m; enclosure depth – 0.225 m, 0.325 m, 0.425 m; thermal resistance of the heat pipes – 0.01 K/W, 0.1 K/W, 1 K/W.

The range of variable parameters was selected taking into account the availability of a wide range of enclosure materials. The height and depth of the enclosure were varied in order to determine trends in their influence on the thermal mode of the heat pipe enclosure. Changing the thermal resistance by a factor of 100 effectively defines the boundaries of heat pipe application. $P_H = 0.01$ K/W – the operating limit for heat pipes with high heat transfer efficiency, and $P_H = 1$ K/W – actual operation without heat pipes.

It was proven that for a low-temperature compartment size of: height – 0.160 m, width – 0.385 m, depth – 0.225 m, the installation of heat pipes equalizes temperatures to within 0.2 °C. The system reaches operating mode approximately 20% faster.

An increase in enclosure depth from 0.225 m to 0.425 m reduces the effectiveness of heat pipes by 45%, and an increase in height from 0.160 m to 0.280 m reduces their efficiency by 2.6%.

For developers of absorption thermotransformers models with an low-temperature compartment useful volume of 12 – 30 dm³ and refrigeration chamber – of 100 – 180 dm³, the recommended enclosure configuration is with dimensions of 0.160×0.225×0.385 m and with L-shaped or U-shaped heat pipes. The working fluid is ammonia.

Conclusions

1. A mathematical model of the thermal scheme “absorption thermotransformers evaporator – heat pipe – low-temperature compartment” has been developed, enabling numerical experiments to assess the influence of the following geometric and operational parameters on the thermal and energy characteristics of the absorption thermotransformers, specifically the low-temperature compartment enclosure: depth, width, and height of the low-temperature compartment enclosure; material thickness; type of enclosure material; type of heat pipe used, taking into consideration thermal resistance value; and thickness of insulation barriers.

2. The study demonstrates the feasibility and advantages of using heat pipes of various configurations – particularly L-shaped and U-shaped designs.

Література

1. UNEP. Montreal Protocol on Substances That Deplete the Ozone Layer. Final Act. 1987. 11 September. URL: https://ozone.unep.org/treaties/montreal-protocol.
2. Srikhirin P., Aphornratana S., Chungpaibulpatana S. A review of absorption refrigeration technologies. *Renewable and Sustainable Energy Reviews*. 2001. № 5. P. 343–372.
3. Talpada J., Ramana P. A review on performance improvement of an absorption refrigeration system by modification of basic cycle. *International Journal of Ambient Energy*. 2017. No. 6, Vol. 40. P. 661–673. DOI: https://doi.org/10.1080/01430750.2017.1423379.
4. Xi Wu, Shiming Xu, Mengnan Jiang. Development of bubble absorption refrigeration technology: A review. *Renewable and Sustainable Energy Reviews*. 2018. Vol. 82, Part. 3. P. 3468–3482. DOI: https://doi.org/10.1016/j.rser.2017.10.109.
5. Afshar O. et al. A review of thermodynamics and heat transfer in solar refrigeration system. *Renewable and Sustainable Energy Reviews*. 2012. No. 8, Vol. 16. P. 5639–5648. DOI: https://doi.org/10.1016/j.rser.2012.05.016.
6. Busso A. et al. Attempt of integration of a small commercial ammonia-water absorption refrigerator with a solar concentrator: Experience and results. *International Journal of Refrigeration*. 2011. No. 8, Vol. 34. P. 1760–1775. DOI: https://doi.org/10.1016/j.ijrefrig.2011.07.004.
7. Chen J., Kim K., Herold K. Performance enhancement of a diffusion-absorption refrigerator. *International Journal of Refrigeration*. 1996. No. 3, Vol. 19. P. 208–218. DOI: https://doi.org/10.1016/0140-7007(96)87215-X.
8. Adjibade M. et al. Dynamic investigation of the diffusion absorption refrigeration system NH3-H2O-H2. *Case Studies in Thermal Engineering*. 2017. № 10. P. 468–474. DOI: https://doi.org/10.1016/j.csite.2017.10.006.
9. A numerical investigation of a diffusion absorption refrigerator operating with the binary refrigerant for low temperature applications / Wang Q., Gong L., Wang J.P., Sun T.F., Cui K., Chen G.M. *Applied Thermal Engineering*. 2011. № 10, Vol. 31. P. 1763–1769. DOI: https://doi.org/10.1016/j.applthermaleng.2011.02.021.
10. Titlova O., Titlov O., Olshevska O. Searching for the energy efficient operation modes of absorption refrigeration devices. *Eastern-European Journal of Enterprise Technologies*. 2016. 5 (83). P. 45–53. DOI: https://doi.org/10.15587/1729-4061.2016.79353.
11. Дюженкова Л.І., Носаль Т.В. *Вища математика: практикум*: навч. посібник. Київ : Вища школа, 1991. 407 с. ISBN: 5-11-002281-X.
12. Лабай В. Й. *Тепломасообмін*. Львів: Тріада Плюс, 1998. 260 с.
13. Bilenko N., Titlov O. Improving energy efficiency of the systems for obtaining water from atmospheric air. *Eastern-European Journal of Enterprise Technologies*. 2021. 2/8 (110). P. 31–40. DOI: https://doi.org/10.15587/1729-4061.2021.229545.
14. Study of the effect of tilt angle on the vaporization processes in a flat gravity heat pipe with a threaded evaporator / Nikolaenko Yu.E., Melnyk R.S., Lipnitsky L.V., Kravets V.Yu., Pekur D.V. *Journal of Thermal Analysis and Calorimetry*. 2023. Vol. 148, Issue 12. P. 9167–9181. DOI: https://doi.org/10.1007/s10973-023-12303-0.
15. Comparison of thermal characteristics of three modifications of gravity heat pipe with threaded evaporator at different inclination angles / Pekur D.V., Nikolaenko Yu.E., Kravets V.Yu., Kozak D.V., Sorokin V.M., Nikolaienko T.Yu. *Thermal Science and Engineering Progress*. 2023. Vol. 46. Art. 102219. DOI: https:// doi.org/10.1016/j.tsep.2023.102219.

References

1. UNEP. (1987). *Montreal Protocol on Substances That Deplete the Ozone Layer. Final Act*. Retrieved from https://ozone.unep.org/treaties/montreal-protocol.
2. Srikhirin, P., Aphornratana, S., & Chungpaibulpatana, S. (2001). A review of absorption refrigeration technologies. *Renewable and Sustainable Energy Reviews, 5*, 343–372.
3. Talpada, J., & Ramana, P. (2017). A review on performance improvement of an absorption refrigeration system by modification of basic cycle. *International Journal of Ambient Energy, 40*(6), 661–673. DOI: https://doi.org/10.1080/01430750.2017.1423379.

ISSN 2076-2429 (print)
ISSN 2223-3814 (online)

4. Wu, X., Xu, S., & Jiang, M. (2018). Development of bubble absorption refrigeration technology: A review. *Renewable and Sustainable Energy Reviews*, *82*(Part 3), 3468–3482. DOI: https://doi.org/10.1016/j.rser.2017.10.109.
5. Afshar, O., Tahmasebi, N., & Ghodsizadeh, A. R. (2012). A review of thermodynamics and heat transfer in solar refrigeration system. *Renewable and Sustainable Energy Reviews*, *16*(8), 5639–5648. DOI: https://doi.org/10.1016/j.rser.2012.05.016.
6. Busso, A., Costa, P., Giordana, F., & Mauran, S. (2011). Attempt of integration of a small commercial ammonia-water absorption refrigerator with a solar concentrator: Experience and results. *International Journal of Refrigeration*, *34*(8), 1760–1775. DOI: https://doi.org/10.1016/j.ijrefrig.2011.07.004.
7. Chen, J., Kim, K., & Herold, K. (1996). Performance enhancement of a diffusion-absorption refrigerator. *International Journal of Refrigeration*, *19*(3), 208–218. DOI: https://doi.org/10.1016/0140-7007(96) 87215-X.
8. Adjibade, M., Lévêque, G., & Auriol, F. (2017). Dynamic investigation of the diffusion absorption refrigeration system NH3-H2O-H2. *Case Studies in Thermal Engineering*, *10*, 468–474. DOI: https://doi.org/10.1016/j.csite.2017.10.006.
9. Wang, Q., Gong, L., Wang, J. P., Sun, T. F., Cui, K., & Chen, G. M. (2011). A numerical investigation of a diffusion absorption refrigerator operating with the binary refrigerant for low temperature applications. *Applied Thermal Engineering*, *31*(10), 1763–1769. DOI: https://doi.org/10.1016/j.applthermaleng.2011.02.021.
10. Titlova, O., Titlov, O., & Olshevska, O. (2016). Searching for the energy efficient operation modes of absorption refrigeration devices. *Eastern-European Journal of Enterprise Technologies*, *5*(83), 45–53. DOI: https://doi.org/10.15587/1729-4061.2016.79353.
11. Dyuzhenkova, L. I., & Nosal, T. V. (1991). *Higher Mathematics: Practical Course*. Higher School.
12. Labai, V. Y. (1998). *Heat and mass transfer*. Triada Plus.
13. Bilenko, N., & Titlov, O. (2021). Improving energy efficiency of the systems for obtaining water from atmospheric air. *Eastern-European Journal of Enterprise Technologies*, *2*(8), 31–40. DOI: https://doi.org/ 10.15587/1729-4061.2021.229545.
14. Nikolaenko, Y. E., Melnyk, R. S., Lipnitsky, L. V., Kravets, V. Y., & Pekur, D. V. (2023). Study of the effect of tilt angle on the vaporization processes in a flat gravity heat pipe with a threaded evaporator. *Journal of Thermal Analysis and Calorimetry*, *148*(12), 9167–9181. DOI: https://doi.org/10.1007/s10973-023-12303-0.
15. Pekur, D. V., Nikolaenko, Y. E., Kravets, V. Y., Kozak, D. V., Sorokin, V. M., & Nikolaienko, T. Y. (2023). Comparison of thermal characteristics of three modifications of gravity heat pipe with threaded evaporator at different inclination angles. *Thermal Science and Engineering Progress*, *46*, 102219. DOI: https://doi.org/10.1016/j.tsep.2023.102219.

Тітлов Олександр Сергійович; Oleksandr Titlov, ORCID: http://orcid.org/0000-0003-1908-5713
Пономарьов Костянтин Миколайович; Konstantin Ponomaryov, ORCID: https://orcid.org/0000-0002-7771-1316

Received April 03, 2025
Accepted May 16, 2025